Nonreciprocal microwave field transmission in a quantum magnomechanical system controlled by magnetostriction and Kerr nonlinearities

Muhib Ullah[1] and Said Mikki [1,2,*]

[1]*Zhejiang University/University of Illinois Urbana-Champaign* (ZJU-UIUC) Institute,
Zhejiang University, International Campus, Haining, Zhejiang 314400, China
[2]*Electrical and Computer Engineering Department, University of Illinois Urbana-Champaign*, Urbana, Illinois 61801, USA

We theoretically demonstrate nonreciprocity in signal transmission within a three-mode system by exploiting the nonlinear magnetostrictive interaction within a ferrimagnetic material enclosed in a magnomechanical cavity system. This setup encompasses two cavity modes: a magnonic mode and phononic modes. Externally, it is driven by two classical microwave fields: a strong driving magnetic field and a weak probe field. In the cavity setup, a yttrium iron garnet sphere is subjected to a strong magnetic field, significantly affecting the spins within the sphere and leading to deformations in its geometry. These deformations, in turn, induce phonon modes within the sphere. Moreover, three distinct types of nonlinearities are triggered: magnetostriction, magnon self-Kerr, and magnon-phonon cross-Kerr nonlinearities. Additionally, magnons interact with cavity microwave photons through a magnetic dipole interaction. The nonlinear magnetostrictive interaction induces a phase shift in the cavity's photons, causing the breaking of time-reversal symmetry and ultimately resulting in the observed nonreciprocal phenomenon in our hybrid magnomechanical cavity system. Furthermore, by adjusting the magnetostrictive interaction, we can achieve maximal nonreciprocal signal transmission at either port. These results also encompass the significance of the magnon dissipation rate while realizing its nonreciprocity. The detunings of all three modes, that is, two microwave photonic modes and a magnonic mode, are found to be critical for fine tuning the process of nonreciprocal transmission and modulating its characteristics. Since the proposed setup is quite simple, tunable, and experimentally realizable, the proposed configuration and related outcomes could be utilized for applications in quantum communication networks and quantum computing, boost up the sensitivity of microwave detectors, and contribute to advancements in circulators, switching, and other quantum information processing tasks.

I. INTRODUCTION

Nonreciprocal devices have captured significant attention within the engineering and physics communities, owing to their broad applicability in fields like invisible sensing and signal processing, which encompass functionalities such as isolators and directional amplifiers [1]. The manifestation of the nonreciprocal effect occurs when these devices disturb time-reversal symmetry. Traditional nonreciprocal devices rely on magnetic bias fields and the magneto-optic responses of materials [2,3]. Nevertheless, these devices encounter limitations due to weak magneto-optic coefficients. In response to these constraints, several alternative approaches have been recently proposed to supplant traditional schemes. These alternatives include techniques such as incorporating angular momentum biasing in photonic or phononic crystals, leveraging the quantum Hall effect, implementing synthetic magnetism, harnessing optical nonlinearity, exploring optomechanical interactions, and others [4–11].

In recent years, there has been an increasing interest in exploring ferromagnetic materials to investigate fundamental quantum physics concepts and implement quantum information protocols [12–16]. Researchers are actively engaged in manipulating the interactions between acoustic waves, also known as phonons, and the collective spins in ferromagnetic materials, specifically magnons. This area of study, known as magnomechanics, has gained significant attention for its important applications and contributions to quantum information processing [17–28]. Particularly, cavity magnomechanics represents an emerging field of study in which the phonons are effectively confined within a cavity inside the magnetic material, thus leading to a significant enhancement of the magnetostrictive or magnon-phonon coupling. This cavity-based enhancement introduces various features that include coherent conversion of energy between magnons and phonons [29–31], controlling the dynamical back-action [32], back-action-evading measurements [30,31], and the realization of magnetic material-based mechanical bistability [33]. The initial work utilized a sphere constructed from a yttrium iron garnet (YIG), in which a phononic mode oscillating radially interacts with a collective magnetization excitation referred to as the Kittel mode [29,31]. The YIG sphere possesses desirable characteristics, including high spin density, with extremely low magnon loss and damping rate [34], and a high Curie temperature [35,36]. The study presented here will

----
*Contact author: smikki@illinois.edu

not only contribute to practical outcomes, but also has the potential to inspire the conceptualization of control protocols, as evidenced by research papers such as [37–39]. Moreover, our approach draws analogies to control methodologies in cavity quantum electrodynamics (QED) [40] and cavity optomechanics [10].

The interaction between magnons in a YIG crystal and microwave photons in a superconducting resonator has been demonstrated to reach the regimes of strong and ultrastrong coupling. Particularly, the Kittel mode [41] in the YIG sphere can achieve strong coupling with the microwave photons in a high-Q-factor cavity, leading to the formation of cavity polaritons [14,36,42–44]. This coupling strength is enhanced by a factor of the square root of the number of spins involved ($\sqrt{N}$) and is independent of the number of magnons inside the YIG sphere. Quantum applications in this field have been realized experimentally, including the observation of the magnon Kerr effect [45], the identification of magnon dark modes [46], the observation of bistability in cavity magnon polaritons [47], the detection of single magnons [48], and nonreciprocal microwave transmission [49–52].

The nonreciprocal behavior of the spin wave in a magnetic material has been realized experimentally in addition to being investigated theoretically [53,54]. In the cavity magnomechanical system, several scientists have achieved unidirectional invisibility by employing both coherent and dissipative magnetic dipole moments of the cavity-magnon couplings [49,55], while nonreciprocal transmission based on the magnon Kerr effect has been explored [50]. In a recent investigation, a method was proposed to produce entanglement between two microwave fields by employing the nonlinear magnetostrictive interaction inherent in a YIG material [56]. The magnetostrictive interaction enables the coupling between a magnon mode (a collective spin wave) and a mechanical mode within the YIG sphere. The findings are derived from steady-state solutions of the system variables under study. More recently, Zhao *et al.* have studied a hybrid model containing two cavities with two YIG spheres enclosed where they have theoretically investigated nonreciprocity of output signals with amplification [57].

The nonlinearity observed in magnetic materials emerges when the YIG sphere is subjected to a strong drive field. Two significant nonlinearities, namely, the magnon self-Kerr and cross-Kerr nonlinearities, along with the inherent magnetostrictive interactions, contribute to this phenomenon. These nonlinearities have the capability to effectively shift the optical, magnetic (magnon), and mechanical frequencies, thereby altering the system's dynamics. Experimental demonstrations of the magnon Kerr effect have been conducted in strongly coupled cavity-magnon systems. In these systems, the Kerr effect leads to a shift in the cavity's central frequency and induces more pronounced shifts in the magnon modes [31,32,45]. Unlike the influence of a strong external field, Kerr nonlinearity can substantially modify the dynamics through the deployment of relatively weak drive fields [31,58,59].

Inspired by this development, we study nonreciprocity within a hybrid multimode magnomechanical system. This system features two microwave cavity fields connected to the magnon mode of a YIG sphere through a magnetic dipole moment. Our primary objective in this study is to explore the generation, manipulation, and control of nonreciprocal signal transmission. The magnon mode engages magnetostrictively with the phonon produced by the collective magnetic spin, induced by the excitation of the YIG sphere through an external magnetic drive field. Additionally, Kerr nonlinearties (self-Kerr and cross-Kerr) are activated when the YIG sphere is excited by a strong drive. The two microwave cavity modes can directly transfer microwave photons to each other through photon-hopping interactions. Very recently, nonreciprocal photon blockade has been investigated in a single-cavity magnomechanical system having two YIG spheres in which the nonreciprocity is controlled via tuning Kerr nonlinearities [60]. Going beyond steady-state solutions, we perturb the system dynamics by introducing a weak probe field to both microwave cavity modes, and operate the system to impart nonreciprocity to the signals flowing in the opposite direction. Normally, the Kerr nonlinearities and magnetostrictive interaction between magnon and phonon are weak, but using the specific system under study, the YIG sphere is excited via an external drive magnetic field which efficiently enhances the spin waves inside and thus phonons can be created effectively that couple with magnons via magnetostrictive interaction. A phase difference between distinct field paths can be manipulated either by tuning the external magnetic field or by displacing the YIG sphere within the cavity setup. Ultimately, adjusting the system parameters to introduce a substantial phase difference can result in the breaking of time-reversal symmetry, paving the way for achieving nonreciprocal transmission of information.

The paper's structure is outlined as follows: Section II elucidates the model of the proposed system and addresses the solution to the system's Hamiltonian. Section III provides numerical results pertaining to nonreciprocity and some additional related discussions. The concluding remarks of our work are presented in the last section.

II. SYSTEM MODEL AND ANALYTICAL RESULTS

The schematic representation of the proposed scheme's general magnomechanical system model is presented in Fig. 1. This model encompasses a magnon mode m within a YIG sphere, which interacts with two microwave cavity modes or fields a_1 and a_2 through magnetic dipole interactions denoted as g_1 and g_2, respectively. Additionally, the magnon mode is connected to the mechanical oscillation or phonon mode b via magnetostrictive interaction G_s. The YIG sphere is subjected to the influence of a robust magnetic field with a strength denoted as Ω and frequency ω_d to maintain the strength of the magnetostrictive interaction. The resulting output field can be collected at both output ports 1 and 2, respectively. Moreover, the two cavities experience a photon-hopping interaction characterized by a hopping coupling denoted as J.

Applying the unitary transformation $U(t) = \exp[-i\omega_d(a_i^\dagger a_i + m^\dagger m)t]$ $(i = 1, 2)$ (analogous to the Schrödinger equation) in the frame rotating at the magnetic
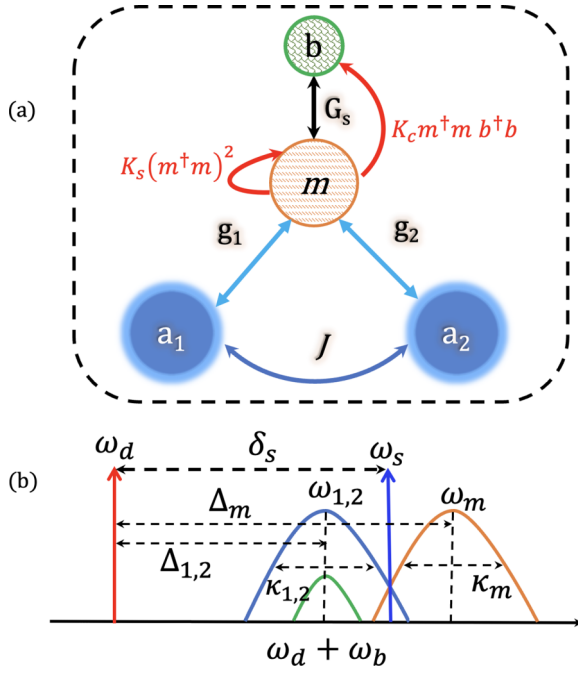
FIG. 1. (a) Conceptual framework for the magnomechanical system under consideration. A magnon excitation denoted as m within a yttrium iron garnet (YIG) sphere interacts with two distinct microwave cavity modes a_1 and a_2 via magnetic dipole couplings g_1 and g_2, respectively, and engages with a phononic mode b through a magnetostrictive coupling G_s. The red curved arrows show the self-Kerr and cross-Kerr nonlinearities with K_s and K_c as their Kerr coefficients, respectively [58]. (b) Spectral characteristics, detuning parameters, and decay constants. The magnonic excitation within the YIG resonator, with a natural frequency ω_m, is excited by a strong microwave drive of amplitude Ω and frequency ω_d. This interaction leads to the generation of phonons at frequency ω_b due to the coherent spin dynamics of magnons in the YIG material. Both cavities are subjected to weak external probe fields at frequency ω_s and are interconnected directly through a photonic-hopping interaction J.

drive frequency, the system Hamiltonian undergoes transformation, as indicated by the expression

$$H_T/\hbar = \sum_{i=1}^{2} \Delta_i a_i^\dagger a_i + \Delta_m m^\dagger m + \omega_b b^\dagger b + G_s m^\dagger m (b^\dagger + b)$$
$$+ g_1(a_1 m^\dagger e^{-i\phi} + a_1^\dagger m e^{i\phi}) + g_2(a_2 m^\dagger + a_2^\dagger m)$$
$$+ i\Omega(m^\dagger - m) + J(a_1^\dagger a_2 + a_2^\dagger a_1) + K_s(m^\dagger m)^2$$
$$+ K_c m^\dagger m b^\dagger b + i \sum_{l=1}^{2} \Omega_{sl}(a_l^\dagger e^{-i\delta_s t} - a_l e^{i\delta_s t}), \quad (1)$$

where $\Delta_1 = \omega_{a1} - \omega_d$ and $\Delta_2 = \omega_{a2} - \omega_d$ are the cavity-drive field detunings, whereas $\Delta_m = \omega_m - \omega_d$ is the magnon-drive field detuning. The Rabi frequency $\Omega = (\sqrt{5}/4)\gamma_0\sqrt{N_s}B_0$ denotes the coupling strength between the magnon mode and its driving magnetic field with amplitude B_0 while N_s is the total number of spins, carrying the expression $N_s = \rho V$ with the spin density of YIG $\rho = 4.22 \times 10^{27}$ m^{-3} and the volume of sphere V [37]. The gyromagnetic

ratio γ_0 relates the magnetic moment of the spin to the applied magnetic field and has a value $\gamma_0/2\pi = 28$ GHz/T.

The first term in (1) represents the Hamiltonian for two cavity modes with Δ_i ($i = 1, 2$) as their detunings. The second term accounts for the energy of the magnon mode with Δ_m representing the magnon's detuning. (Magnons, quantized spin waves, arise as collective excitations of a large number of spins within a massive YIG sphere.) The third term delineates the Hamiltonian for the phonon mode induced by the oscillations of the YIG sphere, where ω_b represents the resonance frequency of the phonon. The subsequent term establishes the coupling between the magnon and phonon modes through the magnetostrictive interaction, involving $b^\dagger$ and b as the creation and annihilation operators of the phonon, respectively. Here, G_s denotes the magnetostrictive coupling strength between the magnon and phonon. The expressions $g_1(a_1 m^\dagger e^{-i\phi} + a_1^\dagger m e^{i\phi})$ and $g_2(a_2 m^\dagger + a_2^\dagger m)$, representing the fifth and sixth terms, describe the magnetic dipole interactions occurring between two microwave cavity photon modes and the magnon mode. In these expressions, g_1 and g_2 denote the coupling rates between the magnon mode and the respective cavity modes a_1 and a_2. The total phase difference, which arises due to the nonlinear characteristics of the YIG sphere, is denoted by ϕ. Importantly, these coupling rates can be much larger than the dissipation rates of the cavity and magnon modes, i.e., $g_i \gg \kappa_i, \kappa_m$ in certain cases, resulting in the formation of cavity-magnon polaritons. The subsequent expression in Eq. (1) corresponds to the hopping interaction between the two cavity modes, with J representing the hopping coupling [61]. In the given context, assuming general applicability, the magnetic dipole moment couplings g_1 and g_2, along with the photon-hopping coupling J, are treated as positive real quantities. Additionally, a total phase difference ϕ is present, which can be derived through a suitable redefinition of the annihilation operators.

The next two terms, i.e., $K_s(m^\dagger m)^2$ and $K_c m^\dagger m b^\dagger b$, represent the self-Kerr and cross-Kerr nonlinearities' Hamiltonians with K_s and K_c as their Kerr coefficients, respectively [33,58]. The concluding term in the Hamiltonian [Eq. (1)] encapsulates the interaction dynamics between the probe field and each of the resonator fields, denoted as a_1 and a_2. Here, $\delta_s = \omega_s - \omega_d$ signifies the detuning between the probe field and the drive field frequencies, while Ω_{sl} represents the amplitude of the probe field.

Adhering to the standard approach in open dynamical systems, we introduce input noise sources and dissipation into the system. Subsequently, the quantum Langevin equation (QLE) is employed to describe the dynamics of the system as follows [62,63]:

$$\frac{dY}{dt} = -\frac{i}{\hbar}[Y, H_T] - \Gamma Y + N, \quad (2)$$

where $Y \in (a_1, a_2, m, b)$ is a general operator variable, Γ is the dissipation rate for each operator under consideration, and the term N denotes a quantum Gaussian white noise whose mean value is zero in the semiclassical approximation [63]. In what follows, the reduced Planck's constant is set to $\hbar = 1$ for convenience. Given our focus on the internal dynamics of the hybrid system, we establish equations of

motion for the observed variables by combining (1) and (2), resulting in

$$\frac{da_1}{dt} = -i\Delta_1 a_1 - ig_1 m e^{i\phi} - iJa_2 - \kappa_1 a_1 + \Omega_{s1} e^{-i\delta_s t}$$
$$+ \sqrt{2\kappa_1} a_1^{in}, \qquad (3)$$

$$\frac{da_2}{dt} = -i\Delta_2 a_2 - ig_2 m - iJa_1 - \kappa_2 a_2 + \Omega_{s2} e^{-i\delta_s t}$$
$$+ \sqrt{2\kappa_2} a_2^{in}, \qquad (4)$$

$$\frac{dm}{dt} = -i\Delta_m m - ig_1 a_1 e^{-i\phi} - ig_2 a_2 - iG_s m(b + b^\dagger)$$
$$- 2iK_s m^\dagger mm - iK_c b^\dagger bm + \Omega - \kappa_m m + \sqrt{2\kappa_m} m^{in}, \qquad (5)$$

$$\frac{db}{dt} = -i\omega_b b - iG_s m^\dagger m - iK_c m^\dagger mb - \gamma_b b + \sqrt{2\gamma_b} b^{in}, \quad (6)$$

where κ_1 and κ_2 are the decay rates of respective microwave cavities, γ_b represents the damping rate of phononic mode, and $\delta_s = \omega_p - \omega_d$ is the probe-drive field detuning.

Due to the robust excitation of the magnon mode, it exhibits a significantly large amplitude, denoted as $|\langle m \rangle| \gg 1$. Concurrently, the cavity-magnon beam-splitter-like interactions result in substantial amplitudes for the two cavity fields. This scenario facilitates the linearization of the system's dynamics around the semiclassical mean values. We represent each mode operator as the sum of its semiclassical averages and for quantum fluctuations, represented as $Z = \langle Z \rangle + \delta Z$ where Z stands for and element of the set $\{a_1, a_2, m, b\}$ [63–65]. In this formulation, we disregard the smaller terms of second-order fluctuations. Upon integrating these linearized mode operators into Eqs. (3)–(6), we can bifurcate the equations into two distinct groups: one describing the semiclassical average behaviors and the other focusing on the quantum fluctuations. The solutions to the averages $\langle Z \rangle = Z_s$ can be expressed as

$$a_{1s} = -\eta(Jg_2 + ig_1 e^{i\phi} \Delta_2')m_s, \qquad (7)$$

$$a_{2s} = -\eta(Jg_1 e^{i\phi} + ig_2 \Delta_1')m_s, \qquad (8)$$

$$|m_s|^2 = \frac{\Omega^2}{\left[\kappa_m + \eta(g_1^2 \Delta_2' + g_2^2 \Delta_1')\right]^2 + (\tilde{\Delta}_m - \eta g_1 g_2 J \cos\phi)^2}, \qquad (9)$$

$$(\Omega_b^2 + \gamma_b^2)|b_s|^2 = G_s^2 |m_s|^4, \qquad (10)$$

where $\eta = 1/(J^2 + \Delta_1' \Delta_2')$, $\tilde{\Delta}_m = \Delta_m + 2G_s \text{Re}[b_s] + \chi_{sc}$ represents the effective detuning of the magnon mode being shifted by the magnon self- and cross-Kerr nonlinearities with $\chi_{sc} = 2K_s|m_s|^2 + K_c|b_s|^2$ as mentioned in Refs. [33,58], and $\chi = K_c|m_s|^2$. Here, $\Delta_1' = (\kappa_1 + i\Delta_1)$, $\Delta_2' = (\kappa_2 + i\Delta_2)$, and $\Omega_b = \omega_b + \chi$ is the modified frequency or, in other words, the frequency shift due to cross-Kerr nonlinearity between magnon and phonon. Equation (9) under study is a cubic equation with respect to magnon excitation number $|m_s|^2$, which, after applying the stability conditions under suitable range of drive field, imparts two stable solutions, thus leading to the bistability of magnon and phonon that was already studied in Refs. [33,66].

To demonstrate the influence of quantum fluctuations introduced to the system by weak probe field, we transition to a reference frame that rotates at frequency $\delta_s = \tilde{\Delta}_m = \omega_b$. To facilitate this transformation, we introduce operators that evolve slowly with time, denoted as $\tilde{O}$. Within this new frame, we express the fluctuations in the $\tilde{O} \in \{\delta a_1, \delta a_2, \delta m, \delta b\}$ as [67]

$$\delta a_1 = \delta\tilde{a}_1 e^{-i\delta_s t}, \quad \delta a_2 = \delta\tilde{a}_2 e^{-i\delta_s t}, \quad \delta m = \delta\tilde{m} e^{-i\tilde{\Delta}_m t},$$
$$\delta b = \delta\tilde{b} e^{-i\omega_b t}. \qquad (11)$$

Inserting the ansatz in Eq. (11) into Eqs. (3)–(6) and, after some simplification, we obtain the following equations:

$$\frac{d}{dt}(\delta\tilde{a}_1) = -\Delta_1' \delta\tilde{a}_1 - g_1 \delta\tilde{m} e^{i\phi} - iJ\delta\tilde{a}_2 + \Omega_{s1}, \qquad (12)$$

$$\frac{d}{dt}(\delta\tilde{a}_2) = -\Delta_2' \delta\tilde{a}_2 - g_2 \delta\tilde{m} - iJ\delta\tilde{a}_1 + \Omega_{s2}, \qquad (13)$$

$$\frac{d}{dt}(\delta\tilde{m}) = -\tilde{\Delta}_m' \delta\tilde{m} - iG_m \delta\tilde{b} - ig_1 \delta\tilde{a}_1 e^{-i\phi} - ig_2 \delta\tilde{a}_2, \quad (14)$$

$$\frac{d}{dt}(\delta\tilde{b}) = -\Gamma_b \delta\tilde{b} - iG_m \delta\tilde{m}, \qquad (15)$$

where $\tilde{\Delta}_m' = (\kappa_m + i\tilde{\Delta}_m)$, $\Gamma_b = (\gamma_b + i\Omega_b)$, while $G_m = G_s\langle m \rangle = G_s m_s$ is defined as the effective magnetostrictive coupling between magnon and phonon modes [38]. After simplification, Eqs. (12)–(15) can be put in the following matrix form:

$$\frac{dx}{dt} = Mx(t) + Y(t), \qquad (16)$$

where $x(t) = (\delta\tilde{a}_1 \ \delta\tilde{a}_2 \ \delta\tilde{m} \ \delta\tilde{b})^T$ is a vector of all the operator variables (T denotes the transposition of the matrix), and $Y(t) = (\Omega_{s1} \ \Omega_{s2} \ 0 \ 0)^T$ is the vector of all input fields. The coefficient matrix M can be expanded as follows:

$$M = \begin{pmatrix} -\Delta_1' & -iJ & -ig_1 e^{i\phi} & 0 \\ -iJ & -\Delta_2' & -ig_2 & 0 \\ -ig_1 e^{-i\phi} & -ig_2 & -\tilde{\Delta}_m' & -iG_m \\ 0 & 0 & -iG_m & -\Gamma_b \end{pmatrix}. \qquad (17)$$

By solving for $x(t)$, we derive expressions for $\delta\tilde{a}_1$ and $\delta\tilde{a}_2$ as given below:

$$\delta\tilde{a}_1 = \frac{\eta\Omega_{s2}[\Gamma_b(J\tilde{\Delta}_m' - ig_1 g_2 e^{i\phi}) - G_m^2 J]}{\Gamma_b(\mathbb{Q} + i\tilde{\Delta}_m') + iG_m^2}, \qquad (18)$$

$$\delta\tilde{a}_2 = \frac{\eta\Omega_{s1}[\Gamma_b(J\tilde{\Delta}_m' - ig_1 g_2 e^{-i\phi}) - G_m^2 J]}{\Gamma_b(\mathbb{Q} + i\tilde{\Delta}_m') + iG_m^2}, \qquad (19)$$

where $\mathbb{Q} = \eta Jg_1 g_2 \cos\phi + i\eta(g_1^2 \Delta_2' + g_2^2 \Delta_1')$.

After deriving the adjusted fluctuation coefficients for the two microwave (MW) cavity modes based on the system parameters, we will employ input-output theory. This application of input-output theory enables us to precisely assess the coupling of light into and out of these modes. Such an understanding is fundamental for the purpose of managing and influencing the system dynamics, and it offers a structured framework to characterize both the input and output fields of the system. The general form of this relation outlined in the previous studies is written as [29,68–70]

$$\varepsilon_{\text{out}} + \varepsilon_{\text{in}} = \sqrt{2\kappa}\delta a, \qquad (20)$$
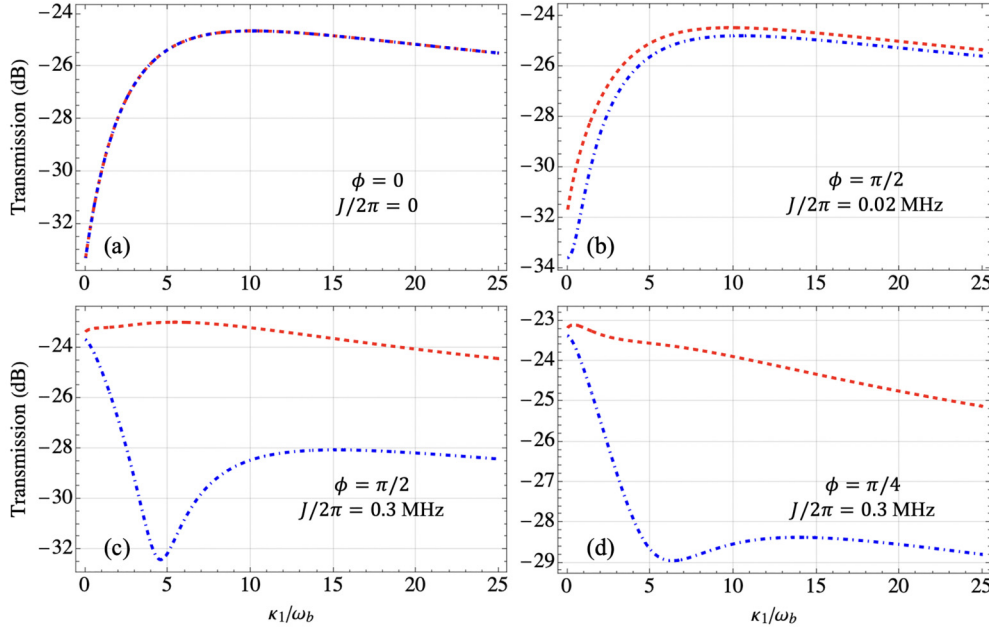
FIG. 2. Transmission of probe signals T_{12} (red curve) and T_{21} (blue curve) plotted against scaled cavity decay rate. The values of the phase and photon-hopping parameters are given as (a) $J = 0$, $\phi = 0$, (b) $J/2\pi = 0.02$ MHz, $\phi = \pi/2$, (c) $J/2\pi = 0.3$ MHz, $\phi = \pi/2$ and (d) $J/2\pi = 0.3$ MHz, $\phi = \pi/4$. The general parameters values used in these numerical results are $\omega_b/2\pi = 15$ MHz, $\Omega = 50\omega_b$, $\Omega_{s1}/2\pi = \Omega_{s2}/2\pi = 0.2\omega_b$, $\kappa_2/2\pi = 1.5$ MHz, $\kappa_m/2\pi = 17.5$ MHz, $\gamma_b/2\pi = 100$ Hz, $g_1/2\pi = g_2/2\pi = 3.5$ MHz, $G_m/2\pi = 2.5$ MHz, $\chi = 0.45\omega_b$, $\chi_s = 0.015\omega_b$, $\chi_c = 0.03\omega_b$ $\omega_m/2\pi = 10$ GHz, $\Delta_m = 0$, and the detunings $\Delta_1 = \Delta_2 = \omega_b$.

where the initial term of Eq. (20) represents the output field, while the subsequent term symbolizes the input field at a specific port. The term on the right-hand side is indicative of the system variable, which encapsulates information about the system's characteristics. In relation to the setup under discussion, the output field, denoted as $\varepsilon_{\text{out}}^1 = \sqrt{\kappa_1}\delta\tilde{a}_1$, corresponds to the microwave photon emission from the microwave mode a_1. This emission occurs under the condition where the input field is in reverse propagation. Similarly, the output field $\varepsilon_{\text{out}}^2 = \sqrt{\kappa_2}\delta\tilde{a}_2$ represents the microwave photon emission from the microwave mode a_2. This emission is observed when the input field is propagating in the forward direction.

We utilize the transmission coefficient expression to characterize and measure the transfer of microwave signals between the two microwave cavity modes with their relations given below:

$$T_{21} \equiv \left|\frac{\varepsilon_{\text{out}}^2}{\Omega_{s1}}\right|, \qquad T_{12} \equiv \left|\frac{\varepsilon_{\text{out}}^1}{\Omega_{s2}}\right|. \tag{21}$$

The numerator of Eq. (21) represents the output while the denominator denotes the input field. By substituting the value of $\delta\tilde{a}_2$ from Eq. (19) into (21), we obtain the final transmission coefficient in the direction from optical mode a_1 to optical mode a_2 is given by

$$T_{21} = \left|\frac{\sqrt{\kappa_1\kappa_2}\,\eta\Omega_{s2}[\Gamma_b(J\tilde{\Delta}'_m - ig_1g_2e^{-i\phi}) - G_m^2 J]}{\Gamma_b(\mathbb{Q} + i\tilde{\Delta}'_m) + iG_m^2}\right|. \tag{22}$$

Similarly, by substituting the value of $\delta\tilde{a}_2$ from Eq. (19) into (21), we calculate the expression for final transmission

coefficient in the opposite direction as follows:

$$T_{12} = \left|\frac{\sqrt{\kappa_1\kappa_2}\,\eta\Omega_{s2}[\Gamma_b(J\tilde{\Delta}'_m - ig_1g_2e^{i\phi}) - G_m^2 J]}{\Gamma_b(\mathbb{Q} + i\tilde{\Delta}'_m) + iG_m^2}\right|. \tag{23}$$

In the upcoming sections, these last two expressions will be extensively utilized to characterize the generation and manipulation of nonreciprocal signal transmission within the proposed magnonic system.

III. RESULTS AND DISCUSSIONS

In this section, we aim to demonstrate the breakdown of time-reversal symmetry, which results in the transition of probe signal transmission from reciprocal to nonreciprocal. The nonreciprocal microwave signal transmission in the system being discussed is primarily governed by two critical factors: the photon-hopping interaction (J) and the total phase difference ϕ across all three modes. This phase difference is introduced into the system due to the nonlinearity of the YIG sphere, which is positioned between two microwave cavity modes. In scenarios where there is an insignificant phase difference, or in the absence of photon hopping, the signal transmission through either port of the system remains reciprocal. Furthermore, the dynamics of the magnomechanical system under analysis is significantly influenced by the external drive magnetic field (strength Ω). This nonreciprocal transmission is intricately linked to the magnetic dipole interactions g_1 and g_2 between the microwave cavity photon modes and the magnon, as well as the magnetostrictive interactions G_s between magnon and phonon.
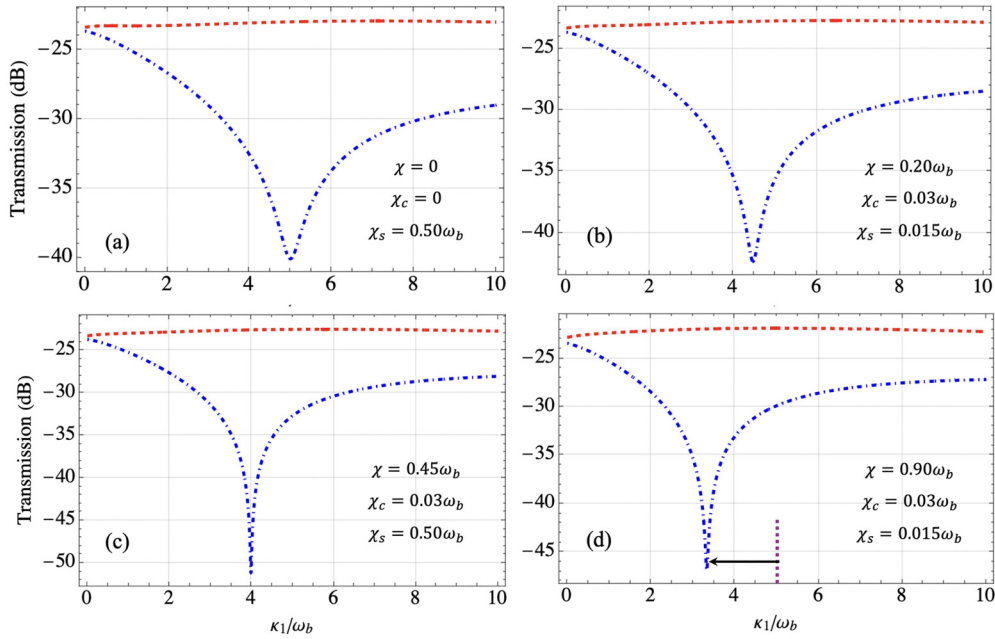
FIG. 3. Output probe signal transmission T_{12} (red curve) and T_{21} (blue curve) plotted against scaled cavity decay rate. The values for the effective self-Kerr and cross-Kerr nonlinearities are given as (a) $\chi = \chi_c = 0$, $\chi_s = 0.50\omega_b$, (b) $\chi = 0.20\omega_b$, $\chi_c = 0.030\omega_b$, $\chi_s = 0.015\omega_b$ (c) $\chi = 0.45\omega_b$, $\chi_c = 0.030\omega_b$, $\chi_s = 0.50\omega_b$, and (d) $\chi = 0.90\omega_b$, $\chi_c = 0.030\omega_b$, $\chi_s = 0.015\omega_b$. The general parameter values used in these numerical results are $\kappa_2/2\pi = 2.8$ MHz, $g_1/2\pi = g_2/2\pi = 3.4$ MHz, $G_m/2\pi = 1.21$ MHz, the magnon detuning $\Delta_m = 3.3\omega_b$, and the phase difference $\phi = 3\pi/2$. Other parameters have same values as given in Fig. 2(c).

In addition to G_s, the setup also includes two other types of nonlinearities: magnon self- and cross-Kerr nonlinearities, which cannot be disregarded under high levels of coupling (see below). Their presence within the setup can effectively alter the magnon detuning $\tilde{\Delta}_m$ and the natural resonance frequency of the phonon ω_b, potentially altering the system's dynamics and consequently the behavior of nonreciprocal signal transmission. For the purpose of conducting numerical simulations, we employ optimal values of parameters that are feasible in experimental setups [47]. These parameters
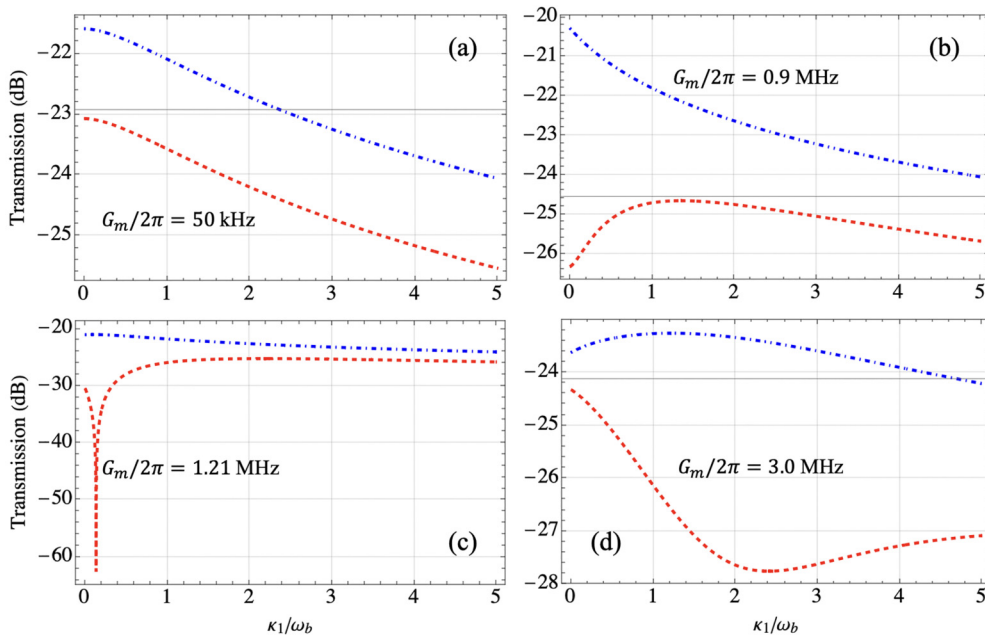
FIG. 4. Transmission of probe signal T_{12} (red dashed curve) and T_{21} (blue dotted-dashed curve) vs cavity decay rate under different values of magnetostrictive interaction: (a) $G_m/2\pi = 50$ kHz, (b) $G_m/2\pi = 0.9$ MHz, (c) $G_m/2\pi = 1.21$ MHz, and (d) $G_m/2\pi = 3.0$ MHz. The general parameters are given as $\kappa_2/2\pi = 2.8$ MHz, $J/2\pi = 0.3$ MHz, $\Delta_m = 3.3\omega_b$, and $\phi = 3\pi/2$. Other parameters are same as given in Fig. 2(c).
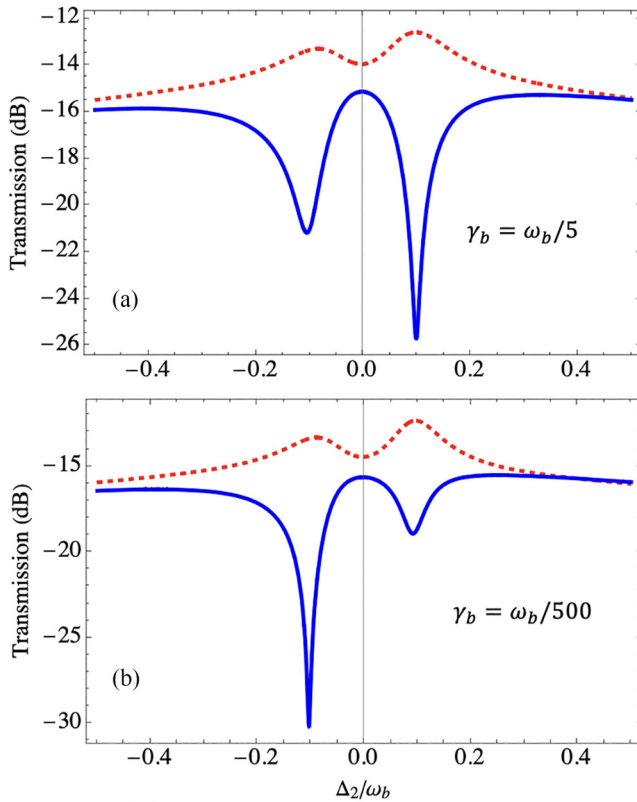
FIG. 5. Output probe signal transmission T_{12} (red dashed curve) and T_{21} (blue dotted-dashed curve) plotted against cavity detuning Δ_2 under different values of phonon damping rate γ_b: (a) $\gamma_b = \omega_b/5$, (b) $\gamma_b = \omega_b/500$. The general parameters are given as $\kappa_2/2\pi = 13.1$ MHz, $\kappa_1 = 0.4\kappa_2$, $\kappa_m/2\pi = 2.5$ MHz, $J/2\pi = 0.8$ MHz, $\Delta_m = \omega_b$, and $\phi = \pi/3$. Other parameters have the same as given in Fig. 2(c).

help in accurately modeling and understanding the complex interplay of photon, magnon, and phonon interactions within the system. The numerical values of system parameters are given as the phonon mode frequency $\omega_b/2\pi = 15$ MHz, the drive field strength $\Omega = 50\omega_b$, input probe field amplitude $\Omega_{s1}/2\pi = \Omega_{s2}/2\pi = 0.2\omega_b$, decay rate of cavity mode 2 $\kappa_2/2\pi = 1.5$ MHz, dissipation rate of magnon mode $\kappa_m/2\pi = 17.5$ MHz, damping rate of phonon mode $\gamma_b/2\pi = 100$ Hz, magnetic dipole interactions $g_1/2\pi = g_2/2\pi = 3.5$ MHz, magnetostrictive interaction $G_m/2\pi = 2.5$ MHz, $\chi = 0.45\omega_b$, $\chi_s = 0.015\omega_b$, $\chi_c = 0.03\omega_b$, magnon resonance frequency $\omega_m/2\pi = 10$ GHz, and the detunings are given as $\Delta_1 = \Delta_2 = \omega_b$, and $\Delta_m = 0$. Given that we deploy relatively strong external drive field, the presence of the three types of nonlinearities, magnetostriction, self-Kerr, and cross-Kerr effects, is unavoidable. Their respective parameter values have been taken into account in the subsequent discussion of the results below.

A. Altering signal transmission via phase shifts and photon hopping

In our exploration of the designated magnomechanical system, we identify two crucial parameters: the phase differential

and the photonic-hopping interaction, both of which play a critical role in modulating the signal's transition from reciprocal to nonreciprocal transmission. As depicted in Fig. 2(a), in the absence of photonic-hopping interaction between the microwave (MW) cavity modes, signal propagation remains strictly reciprocal, evident in the congruence of the blue and red trajectories. The introduction of a significant phase shift ϕ between distinct transmission channels is essential for achieving nonreciprocity. Specifically, when $\phi = \pi/2$, the probe signal's transmission exhibits symmetry in two opposing directions. Figure 2(a) illustrates this reciprocity at both ports, maintaining symmetry regardless of the phase ϕ, particularly when the photonic-hopping coupling J is nullified. The reason that we still do not realize nonreciprocity in our system aside from changing the phase difference is the absence of quantum interference paths among the three modes (microwave cavity mode a_1, a_2, and the magnon mode m inside YIG sphere) are no longer in existence or connection. For interference to happen, the photon hopping must have a nonzero and comparable numerical value to the system parameter values. Upon fine tuning the hopping interaction to $J/2\pi = 0.02$ MHz, we start to observe the emergence of nonreciprocal behavior in the hybrid magnonic structure, as demonstrated in Fig. 2(b), where a noticeable but small bifurcation of the signal paths in opposite directions is observed. However, it is only with an enhanced hopping coupling, at $J/2\pi = 0.3$ MHz, that time-reversal symmetry is decisively disrupted, culminating in a distinctly nonreciprocal microwave signal transmission, an outcome rooted in the quantum interference among diverse transmission paths, as depicted in Fig. 2(c). The dotted-dashed blue trajectories show troughs near $\kappa_1/\omega_b = 5$, indicating reduced transmission at port 2. Simultaneously, the near-flat red crests at the same juncture depict increased transmission at port 1. It is essential to note that maximal nonreciprocity in signal transmission is achieved when the phase parameter is precisely configured to $\phi = \pi/2$ since maximum chances of quantum interference exist to happen at that specific valve of phase. Variations in the phase value, deviating from this optimal point (e.g., $\phi = \pi/4$ in this case), result in a less pronounced nonreciprocal behavior of the signals at both ports, as observed in Fig. 2(d), because of the strong dependency of the transmission routes T_{12} and T_{12} on the phase difference as obvious from Eqs. (22) and (23). From the preceding discussion, it becomes clear that by carefully adjusting the parameters ϕ and J, one can effectively engineer the input signals traversing from diametrically opposed vectors to exhibit nonreciprocal characteristics.

B. Contribution of Kerr nonlinearities in the output transmission

In a magnomechanical system, when a strong external drive field is applied to a magnetic material, such as the YIG sphere in our case, it induces both a radiation pressure, e.g., force and Kerr nonlinearities. These factors collectively influence the system dynamics by altering the resonance frequencies of magnons and phonons, thereby modifying the overall system behavior. Here, we demonstrate the role of the Kerr effect (both self and cross) in manipulating quantum interference, which is responsible for breaking the time-reversal
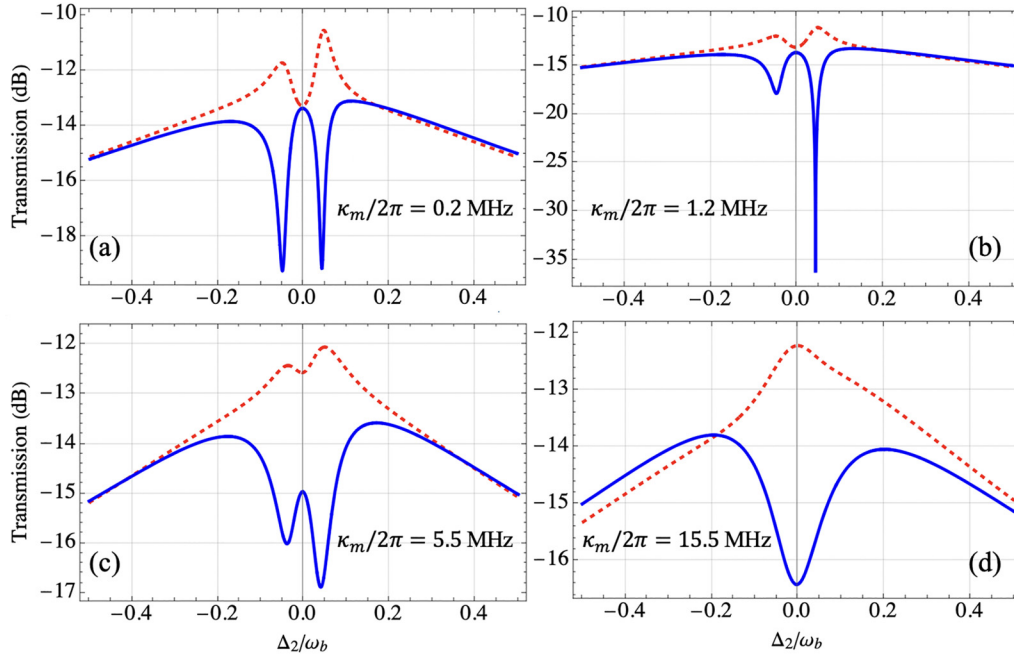
FIG. 6. Output probe signal transmission T_{12} (red dashed curve) and T_{21} (blue dotted-dashed curve) plotted against cavity detuning Δ_2 under different values of magnon dissipation rate κ_m: (a) $\kappa_m/2\pi = 0.2$ MHz, (b) $\kappa_m/2\pi = 1.2$ MHz, (c) $\kappa_m/2\pi = 5.5$ MHz, and (d) $\kappa_m/2\pi = 15.5$ MHz. The general parameters are given as $\kappa_2/2\pi = 6.0$ MHz, $\kappa_1 = 0.4\kappa_2$, $\kappa_m/2\pi = 2.5$ MHz, $J/2\pi = 0.8$ MHz, $\Delta_m = \omega_b$, and $\phi = \pi/3$. Other parameters are same as given in Fig. 2(c).

symmetry, as illustrated in Fig. 3. We provide the values of Kerr coefficients in terms of effective Kerr expressions, such that $\chi = K_c|m_s|^2$, $\chi_s = K_s|m_s|^2$, and $\chi_c = K_c|b_s|^2$. In Fig. 3(a), when $\chi = \chi_c = 0$ and $\chi_s = 0.50\omega_b$, we observe nonreciprocal signal transmission, depicted by a blue curve dip at $\kappa_1/\omega_b = 5$, indicating minimal transmission at port 2. Adjusting the external bias magnetic field to tune the values of Kerr nonlinearities to $\chi = 0.20\omega_b$, $\chi_c = 0.03\omega_b$, and $\chi_s = 0.015\omega_b$, results in a slight shift of the blue dip towards the origin on the frequency axis. The observed shift is attributed to the significant impact of Kerr nonlinearities on magnons and phonons, leading to shifts in their frequencies. These frequency changes cause variations in the total phase ϕ, consequently altering the quantum interference pattern and relocating the position of constructive interference to a new point on the frequency spectrum, as depicted in Fig. 3(c). Additionally, tuning these nonlinearities results in an increase in isolation. A similar type of shift has been experimentally demonstrated in Ref. [33], which investigates shifts in magnomechanically induced resonances, focusing on the self-Kerr nonlinearity. In our current setup, we address both self-Kerr and cross-Kerr nonlinearities, as both significantly contribute to altering the system dynamics. By further adjusting the values of Kerr nonlinearities to $\chi = 0.90\omega_b$, $\chi_c = 0.03\omega_b$, and $\chi_s = 0.015\omega_b$, the dip shift in signal transmission extends further to the left, as indicated by the black arrow, demonstrating the frequency shifts of magnons and phonons from their resonances. From the preceding discussion, it is evident that Kerr nonlinearity plays a crucial role in controlling and manipulating nonreciprocal signal transfer across two ports.

C. Utilizing magnetostrictive interaction to influence signal transmission

In addition to effective Kerr nonlinearities, the effective magnetostrictive coupling, denoted as $G_m = G_s\langle m_s\rangle$, between the magnon and phonon modes under consideration is influenced by the external magnetic drive field strength Ω, which plays a pivotal role in determining the nonreciprocal behavior of microwave (MW) signal transmission. As illustrated in Fig. 4(a), a relatively small magnetostrictive interaction ($G_m/2\pi = 50$ kHz) leads to minimal magnon-induced nonlinearity, thus falling short of achieving optimal nonreciprocal signal transfer. Conversely, increasing G_m to a larger value, for example, $G_m/2\pi = 0.9$ MHz, amplifies the magnetic nonlinearity, thus increasing the magnitude of nonreciprocity of output signals, as depicted in Fig. 4(b). Further elevation of the magnetostrictive coupling to $G_m/2\pi = 1.21$ MHz boosts up the magnitude of nonreciprocal transmission with maximum isolation. This optimal isolation is particularly noticeable around $\kappa_1/\omega_b = 0.1$, where MW signal transmission reaches its peak at port 2 and its minimum at port 1 as illustrated, respectively, by the red trough and blue peak in Fig. 4(c). These findings indicate that increasing G_m shifts the nonreciprocal signal spectrum rightward along the x axis, suggesting that the tunability of nonreciprocal transmission can be effectively controlled through adjustments in magnetostrictive interaction. The shift in the output signal spectrum can be further witnessed by increasing G_m to much higher value, that is, $G_m/2\pi = 3.0$ MHz, where the nonreciprocal signal trajectory spans a broader spectrum along the x axis, as shown in Fig. 4(d). Consequently, it becomes evident that the nonreciprocal MW transmission is intricately dependent on the
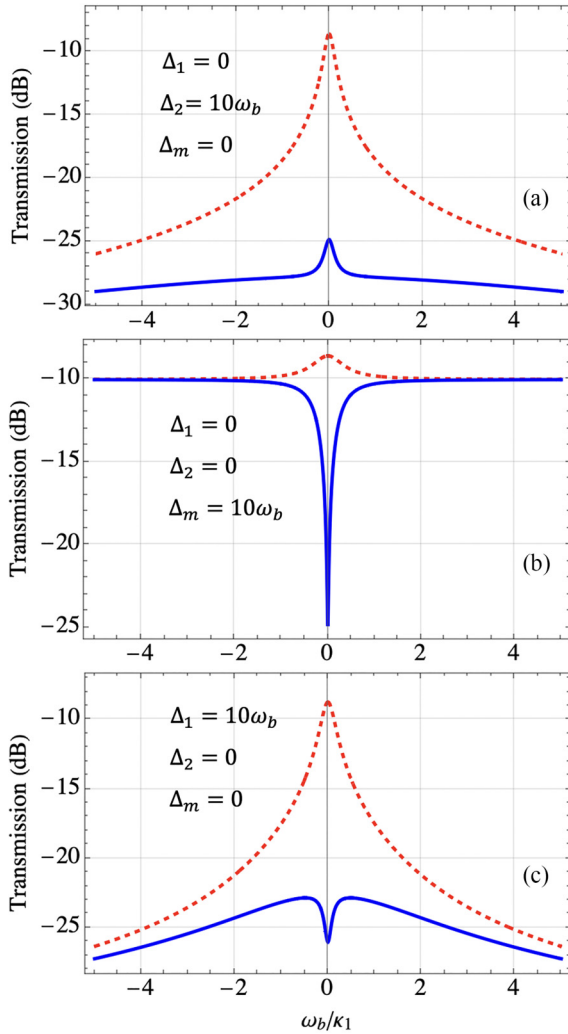
FIG. 7. Output probe signal transmission T_{12} (red dashed curve) and T_{21} (blue dotted-dashed curve) plotted against the phonon frequency ω_b under different system detunings: (a) $\Delta_1 = 0$, $\Delta_2 = 10\omega_b$, $\Delta_m = 0$, (b) $\Delta_1 = 0$, $\Delta_2 = 0$, $\Delta_m = 10\omega_b$, and (c) $\Delta_1 = 10\omega_b$, $\Delta_2 = 0$, $\Delta_m = 0$. The general parameters are given as $\kappa_1 = \kappa_2/2\pi = 6.0$ MHz, $J/2\pi = 0.6$ MHz, $\phi = \pi/2$, $g_1/2\pi = 1.4$ MHz, and $g_2/2\pi = 6.4$ MHz. Other parameters are same as given in Fig. 2(c).

magnitude of magnetostrictive coupling between the magnon and phonon modes. Additionally, the isolation can also be efficiently controlled via tuning of magnetostrictive coupling.

D. Role of phonon damping rate γ_b and magnon decay rate (κ_m) to influence nonreciprocity

Phonons, which are the quantized modes of lattice oscillations, have intrinsic property of damping rate and lose energy to the system by different means. Variation in this damping rate has an incredible impact on the nonreciprocal transmission spectrum. When the phonon loss rate value is considered to be $\gamma_b = \omega_b/5$, the nature of transmission curves of signal at two ports is nonreciprocal as shown in Fig. 5(a), where the right resonance has maximum isolation at $\Delta_2/\omega_b = 0.1$ unlike the curves at the left of origin. The value of phonon loss rate can be reduced to have a better mechanical quality factor. When the value of phonon damping rate

becomes $\gamma_b = \omega_b/500$, the maximal nonreciprocal curve's behavior gets swapped which means that the left curves receive maximal transmission whereas the right one remains short or small as seen in Fig. 5(b). Since, to realize optimal transmission using quantum magnomechanical system, the dissipation or damping should be as least as possible which is quite challenging. But with modern technology techniques, it could be possible to do so by using the optimized materials with intrinsically low damping rates, using cryogenic setups to minimize thermal noise, and incorporating YIG spheres of high purity which reduce inhomogeneous broadening effects on magnon modes, thereby diminishing or minimizing overall losses in the system.

The magnon decay rate, denoted as κ_m, measures the rate of energy dissipation of the magnon and is inversely proportional to its quality factor Q_m, following the relationship $\kappa_m = \omega_m/Q_m$. In this study, we investigate the impact of the magnon decay rate (or, equivalently, the quality factor) on modulating the directionality of signal transmission at the output ports. As depicted in Fig. 6(a), when the magnon decay rate is set to $\kappa_m/2\pi = 0.2$ MHz, the nonreciprocal signal transmission is characterized by dual red peaks and corresponding blue troughs of similar depths at identical points along the frequency axis. This suggests that lower dissipation rates correlate with minimal transmission at port 2 and maximal transmission at port 1. Increasing the dissipation rate to $\kappa_m/2\pi = 1.2$ MHz, as shown in Fig. 6(b), leads to a significantly enhanced depth of the right trough displaying enhanced nonreciprocal transmission at port 1 and minimal at port 2. At this magnitude of the magnon decay rate, optimal quantum constructive interference occurs, leading to a substantial level of isolation. A further increment of the magnon decay rate to $\kappa_m/2\pi = 5.5$ MHz reveals a closure of red peaks and blue troughs towards each other, resulting in lower magnitude of nonreciprocity as can be seen in Fig. 6(c). It becomes clear that higher values of magnon loss rate lower the tendency of optimal transmission at the outputs. It is worthy to mention here that the transmission of signals at the output is always maximum when the leakage, decay, or loss rates inside the system are minimum. The converse happens when the magnon loss rate is set to $\kappa_m/2\pi = 15.5$ MHz as shown in Fig. 6(d). The two peaks and troughs converge into a single peak and trough, respectively, at the origin, resulting in minimal isolation. In the context of nonreciprocity in our proposed setup as explained above in Fig. 6, it is better to keep the magnon dissipation rate as low as possible in order to comply with the quantum magnomechanics. As explained already, for lower values of magnon, decay rate gives optimal magnitude of nonreciprocity as obvious from Fig. 6(b). Higher values of κ_m can still hold the nonreciprocal nature of information signals, but the transmission intensity is reduced as can be seen in Figs. 6(c) and 6(d). Consequently, it can be inferred that the magnon decay rate plays a pivotal role in selectively positioning the nonreciprocal signals along the frequency spectrum.

E. Manipulation of nonreciprocal signal transfer via tuning of detunings

The system under investigation is highly sensitive to the frequencies of various parameters, with their respective

detunings playing a pivotal role in the tunability of nonreciprocal signal transmission. Figure 7 illustrates the effects on nonreciprocal signal transfer when the detunings of both cavities and the magnon are adjusted to distinct values. Initially, we set the detuning of cavity 2 to $\Delta_2 = 10\omega_b$, while reducing the other two detunings, Δ_1 and Δ_m, to zero. This configuration yields nonreciprocal signal propagation, as evidenced by the spatial separation of the two signal curves depicted in Fig. 7(a). Both curves exhibit peaks at the frequency axis origin, indicating an inclination towards increased amplitude. Subsequently, reducing the detunings of both cavities to $\Delta_1 = \Delta_2 = 0$, while adjusting the magnon detuning to $\Delta_m = 10\omega_b$, results in a marked change in the behavior of the blue curve (representing the signal at port 2). It tends towards zero, characterized by a pronounced dip in Fig. 7(b). The signals exhibit a purely nonreciprocal nature with optimal isolation, and the linewidth of the curve is notably narrower compared to that in Fig. 7(a).

Furthermore, with the magnon detuning $\Delta_m = 0$ such that $\omega_m = \omega_d$ and the cavity 1 detuning set to $\Delta_1 = 10\omega_b$, while the cavity 2 detuning is kept zero, i.e., $\Delta_2 = 0$ [as shown in Fig. 7(c)], the linewidth of the signal amplitude at port 1 broadens, peaking at the origin to signify maximum transmission. In contrast, the blue curve (signal at port 2) tends to flatten, exhibiting a minimal dip. By modifying the magnon detuning could potentially render the blue curve entirely flat (not depicted). This analysis underscores the significant influence of frequency detunings on nonreciprocal transmission behavior, demonstrating their potential as a tool for precisely controlling the amount of information transmitted to a desired port.

IV. CONCLUSIONS

In summary, our investigation successfully probed the nonreciprocal behavior of information signals within a hybrid magnomechanical system featuring two microwave (MW) cavity modes interconnected with magnons through magnetic dipole interactions and directly with each other via photon-hopping interaction. By leveraging the inherent nonlinear properties of a yttrium iron garnet (YIG) sphere, we were able to disrupt time-reversal symmetry and control it by adjusting various system parameters. We demonstrated that the breakdown of time-reversal symmetry is contingent upon the presence of a substantial phase difference between all field modes and the cavity modes, coupled with the effect of photon hopping. Manipulation of the relevant nonlinearities, such as magnetostrictive coupling along with self- and cross-Kerr nonlinearities, using an external magnetic field, was found to be pivotal in achieving maximal nonreciprocity and optimal isolation. Additionally, the quality factor of the YIG sphere, as defined by the magnon decay rate, was instrumental in fine tuning the nonreciprocal microwave signal transmission between the two ports. Careful tuning of the detuning parameters allowed us to either inhibit or permit signal transmission through the output ports. In essence, the utilization of hybrid quantum systems incorporating magnetostatic modes presents a wide range of platforms with promising prospects for innovative quantum technologies. These developments bear significance in both foundational and applied physics, unveiling numerous avenues for future research and practical implementation.

[1] D. Jalas, A. Petrov, M. Eich, W. Freude, S. Fan, Z. Yu, R. Baets, M. Popović, A. Melloni, J. D. Joannopoulos *et al.*, What is—and what is not—an optical isolator, Nat. Photonics **7**, 579 (2013).

[2] L. Aplet and J. W. Carson, A faraday effect optical isolator, Appl. Opt. **3**, 544 (1964).

[3] H. Dötsch, N. Bahlmann, O. Zhuromskyy, M. Hammer, L. Wilkens, R. Gerhardt, P. Hertel, and A. F. Popkov, Applications of magneto-optical waveguides in integrated optics, J. Opt. Soc. Am. B **22**, 240 (2005).

[4] D.-W. Wang, H.-T. Zhou, M.-J. Guo, J.-X. Zhang, J. Evers, and S.-Y. Zhu, Optical diode made from a moving photonic crystal, Phys. Rev. Lett. **110**, 093901 (2013).

[5] J.-H. Wu, M. Artoni, and G. C. La Rocca, Non-hermitian degeneracies and unidirectional reflectionless atomic lattices, Phys. Rev. Lett. **113**, 123004 (2014).

[6] G. Viola and D. P. DiVincenzo, Hall effect gyrators and circulators, Phys. Rev. X **4**, 021019 (2014).

[7] L. D. Tzuang, K. Fang, P. Nussenzveig, S. Fan, and M. Lipson, Non-reciprocal phase shift induced by an effective magnetic flux for light, Nat. Photonics **8**, 701 (2014).

[8] X. Guo, C.-L. Zou, H. Jung, and H. X. Tang, On-chip strong coupling and efficient frequency conversion between telecom and visible optical modes, Phys. Rev. Lett. **117**, 123902 (2016).

[9] E. Verhagen and A. Alù, Optomechanical nonreciprocity, Nat. Phys. **13**, 922 (2017).

[10] M. Aspelmeyer, T. J. Kippenberg, and F. Marquardt, Cavity optomechanics, Rev. Mod. Phys. **86**, 1391 (2014).

[11] M. Ullah, X. Yang, and L.-G. Wang, Bidirectional optical non-reciprocity in a multi-mode cavity optomechanical system, Ann. Phys. (Berlin, Ger.) **534**, 2200231 (2022).

[12] N. Arakawa, Stabilizing mechanism for bose-einstein condensation of interacting magnons in ferrimagnets and ferromagnets, Phys. Rev. Lett. **121**, 187202 (2018).

[13] L. Cornelissen, J. Liu, R. Duine, J. B. Youssef, and B. Van Wees, Long-distance transport of magnon spin information in a magnetic insulator at room temperature, Nat. Phys. **11**, 1022 (2015).

[14] L. Bai, M. Harder, Y. Chen, X. Fan, J. Xiao, and C.-M. Hu, Spin pumping in electrodynamically coupled magnon-photon systems, Phys. Rev. Lett. **114**, 227201 (2015).

[15] Y. Li, W. Cao, V. P. Amin, Z. Zhang, J. Gibbons, J. Sklenar, J. Pearson, P. M. Haney, M. D. Stiles, W. E. Bailey *et al.*, Coherent spin pumping in a strongly coupled magnon-magnon hybrid system, Phys. Rev. Lett. **124**, 117202 (2020).

[16] J. Barker and G. E. Bauer, Thermal spin dynamics of yttrium iron garnet, Phys. Rev. Lett. **117**, 217201 (2016).

[17] M. Weiler, L. Dreher, C. Heeg, H. Huebl, R. Gross, M. S. Brandt, and S. T. Gönnenwein, Elastically driven ferromagnetic

resonance in nickel thin films, Phys. Rev. Lett. **106**, 117601 (2011).

[18] L. Dreher, M. Weiler, M. Pernpeintner, H. Huebl, R. Gross, M. S. Brandt, and S. T. Gönnenwein, Surface acoustic wave driven ferromagnetic resonance in nickel thin films: Theory and experiment, Phys. Rev. B **86**, 134415 (2012).

[19] L. Thevenard, C. Gourdon, J.-Y. Prieur, H. J. Von Bardeleben, S. Vincent, L. Becerra, L. Largeau, and J.-Y. Duquesne, Surface-acoustic-wave-driven ferromagnetic resonance in (Ga, Mn)(As, P) epilayers, Phys. Rev. B **90**, 094401 (2014).

[20] T. Kikkawa, K. Shen, B. Flebus, R. A. Duine, K.-i. Uchida, Z. Qiu, G. E. Bauer, and E. Saitoh, Magnon polarons in the spin seebeck effect, Phys. Rev. Lett. **117**, 207203 (2016).

[21] D. Kobayashi, T. Yoshikawa, M. Matsuo, R. Iguchi, S. Maekawa, E. Saitoh, and Y. Nozaki, Spin current generation using a surface acoustic wave generated via spin-rotation coupling, Phys. Rev. Lett. **119**, 077202 (2017).

[22] D. Labanowski, V. P. Bhallamudi, Q. Guo, C. M. Purser, B. A. McCullian, P. C. Hammel, and S. Salahuddin, Voltage-driven, local, and efficient excitation of nitrogen-vacancy centers in diamond, Sci. Adv. **4**, eaat6574 (2018).

[23] R. Sasaki, Y. Nii, and Y. Onose, Surface acoustic wave coupled to magnetic resonance on multiferroic CuB_2O_4, Phys. Rev. B **99**, 014418 (2019).

[24] K. An, A. N. Litvinenko, R. Kohno, A. A. Fuad, V. V. Naletov, L. Vila, U. Ebels, G. de Loubens, H. Hurdequint, N. Beaulieu *et al.*, Coherent long-range transfer of angular momentum between magnon Kittel modes by phonons, Phys. Rev. B **101**, 060407(R) (2020).

[25] A. Hernández-Mínguez, F. Macià, J. Hernàndez, J. Herfort, and P. Santos, Large nonreciprocal propagation of surface acoustic waves in epitaxial ferromagnetic/semiconductor hybrid structures, Phys. Rev. Appl. **13**, 044018 (2020).

[26] P. J. Shah, D. A. Bas, I. Lisenkov, A. Matyushov, N. X. Sun, and M. R. Page, Giant nonreciprocity of surface acoustic waves enabled by the magnetoelastic interaction, Sci. Adv. **6**, eabc5648 (2020).

[27] M. Xu, K. Yamamoto, J. Puebla, K. Baumgaertl, B. Rana, K. Miura, H. Takahashi, D. Grundler, S. Maekawa, and Y. Otani, Nonreciprocal surface acoustic wave propagation via magneto-rotation coupling, Sci. Adv. **6**, eabb1724 (2020).

[28] R. Sasaki, Y. Nii, and Y. Onose, Magnetization control by angular momentum transfer from surface acoustic wave to ferromagnetic spin moments, Nat. Commun. **12**, 2599 (2021).

[29] X. Zhang, C.-L. Zou, L. Jiang, and H. X. Tang, Cavity magnomechanics, Sci. Adv. **2**, e1501286 (2016).

[30] D. Hatanaka, M. Asano, H. Okamoto, Y. Kunihashi, H. Sanada, and H. Yamaguchi, On-chip coherent transduction between magnons and acoustic phonons in cavity magnomechanics, Phys. Rev. Appl. **17**, 034024 (2022).

[31] C. Potts, Y. Huang, V. Bittencourt, S. V. Kusminskiy, and J. Davis, Dynamical backaction evading magnomechanics, Phys. Rev. B **107**, L140405 (2023).

[32] C. A. Potts, E. Varga, V. A. S. V. Bittencourt, S. V. Kusminskiy, and J. P. Davis, Dynamical backaction magnomechanics, Phys. Rev. X **11**, 031053 (2021).

[33] R.-C. Shen, J. Li, Z.-Y. Fan, Y.-P. Wang, and J. You, Mechanical bistability in Kerr-modified cavity magnomechanics, Phys. Rev. Lett. **129**, 123601 (2022).

[34] V. Cherepanov, I. Kolokolov, and V. L'vov, The saga of yig: Spectra, thermodynamics, interaction and relaxation of magnons in a complex magnet, Phys. Rep. **229**, 81 (1993).

[35] D. Zhang, X.-M. Wang, T.-F. Li, X.-Q. Luo, W. Wu, F. Nori, and J. You, Cavity quantum electrodynamics with ferromagnetic magnons in a small yttrium-iron-garnet sphere, npj Quantum Inf. **1**, 15014 (2015).

[36] Y. Tabuchi, S. Ishino, T. Ishikawa, R. Yamazaki, K. Usami, and Y. Nakamura, Hybridizing ferromagnetic magnons and microwave photons in the quantum limit, Phys. Rev. Lett. **113**, 083603 (2014).

[37] J. Li, S.-Y. Zhu, and G. Agarwal, Magnon-photon-phonon entanglement in cavity magnomechanics, Phys. Rev. Lett. **121**, 203601 (2018).

[38] C. Potts, V. A. Bittencourt, S. V. Kusminskiy, and J. Davis, Magnon-phonon quantum correlation thermometry, Phys. Rev. Appl. **13**, 064001 (2020).

[39] T.-X. Lu, H. Zhang, Q. Zhang, and H. Jing, Exceptional-point-engineered cavity magnomechanics, Phys. Rev. A **103**, 063708 (2021).

[40] H. Walther, B. T. Varcoe, B.-G. Englert, and T. Becker, Cavity quantum electrodynamics, Rep. Prog. Phys. **69**, 1325 (2006).

[41] C. Kittel, On the theory of ferromagnetic resonance absorption, Phys. Rev. **73**, 155 (1948).

[42] H. Huebl, C. W. Zollitsch, J. Lotze, F. Hocke, M. Greifenstein, A. Marx, R. Gross, and S. T. Goennenwein, High cooperativity in coupled microwave resonator ferrimagnetic insulator hybrids, Phys. Rev. Lett. **111**, 127003 (2013).

[43] X. Zhang, C.-L. Zou, L. Jiang, and H. X. Tang, Strongly coupled magnons and cavity microwave photons, Phys. Rev. Lett. **113**, 156401 (2014).

[44] M. Goryachev, W. G. Farr, D. L. Creedon, Y. Fan, M. Kostylev, and M. E. Tobar, High-cooperativity cavity qed with magnons at microwave frequencies, Phys. Rev. Appl. **2**, 054002 (2014).

[45] Y.-P. Wang, G.-Q. Zhang, D. Zhang, X.-Q. Luo, W. Xiong, S.-P. Wang, T.-F. Li, C.-M. Hu, and J. You, Magnon Kerr effect in a strongly coupled cavity-magnon system, Phys. Rev. B **94**, 224410 (2016).

[46] X. Zhang, C.-L. Zou, N. Zhu, F. Marquardt, L. Jiang, and H. X. Tang, Magnon dark modes and gradient memory, Nat. Commun. **6**, 8914 (2015).

[47] Y.-P. Wang, G.-Q. Zhang, D. Zhang, T.-F. Li, C.-M. Hu, and J. You, Bistability of cavity magnon polaritons, Phys. Rev. Lett. **120**, 057202 (2018).

[48] S. P. Wolski, D. Lachance-Quirion, Y. Tabuchi, S. Kono, A. Noguchi, K. Usami, and Y. Nakamura, Dissipation-based quantum sensing of magnons with a superconducting qubit, Phys. Rev. Lett. **125**, 117701 (2020).

[49] Y.-P. Wang, J. Rao, Y. Yang, P.-C. Xu, Y. Gui, B. Yao, J. You, and C.-M. Hu, Nonreciprocity and unidirectional invisibility in cavity magnonics, Phys. Rev. Lett. **123**, 127202 (2019).

[50] C. Kong, H. Xiong, and Y. Wu, Magnon-induced nonreciprocity based on the magnon Kerr effect, Phys. Rev. Appl. **12**, 034001 (2019).

[51] N. Zhu, X. Han, C.-L. Zou, M. Xu, and H. X. Tang, Magnon-photon strong coupling for tunable microwave circulators, Phys. Rev. A **101**, 043842 (2020).

[52] C. Kong, X.-M. Bao, J.-B. Liu, and H. Xiong, Magnon-mediated nonreciprocal microwave transmission based on quantum interference, Opt. Express **29**, 25477 (2021).

[53] A. Sadovnikov, E. Beginin, S. Sheshukova, Y. P. Sharaevskii, A. Stognij, N. Novitski, V. Sakharov, Y. V. Khivintsev, and S. Nikitov, Route toward semiconductor magnonics: Light-induced spin-wave nonreciprocity in a YIG/GaAs structure, Phys. Rev. B **99**, 054424 (2019).

[54] S. Odintsov, S. Sheshukova, S. Nikitov, E. Lock, E. Beginin, and A. Sadovnikov, Nonreciprocal spin wave propagation in bilayer magnonic waveguide, J. Magn. Magn. Mater. **546**, 168736 (2022).

[55] Y. Zhao, J. Rao, Y. Gui, Y. Wang, and C.-M. Hu, Broadband nonreciprocity realized by locally controlling the magnon's radiation, Phys. Rev. Appl. **14**, 014035 (2020).

[56] M. Yu, H. Shen, and J. Li, Magnetostrictively induced stationary entanglement between two microwave fields, Phys. Rev. Lett. **124**, 213604 (2020).

[57] C. Zhao, R. Peng, Z. Yang, S. Chao, C. Li, Z. Wang, and L. Zhou, Nonreciprocal amplification in a cavity magnonics system, Phys. Rev. A **105**, 023709 (2022).

[58] V. Bittencourt, C. Potts, Y. Huang, J. Davis, and S. V. Kusminskiy, Magnomechanical backaction corrections due to coupling to higher-order walker modes and Kerr nonlinearities, Phys. Rev. B **107**, 144411 (2023).

[59] R. Hou, W. Zhang, X. Han, H.-F. Wang, and S. Zhang, Magnon blockade based on the Kerr nonlinearity in cavity electro-magnonics, Phys. Rev. A **109**, 033721 (2024).

[60] X.-H. Fan, Y.-N. Zhang, J.-P. Yu, M.-Y. Liu, W.-D. He, H.-C. Li, and W. Xiong, Nonreciprocal unconventional photon blockade with Kerr magnons, Adv. Quantum Technol. (to be published).

[61] E. Russo, A. Mercurio, F. Mauceri, R. Lo Franco, F. Nori, S. Savasta, and V. Macrì, Optomechanical two-photon hopping, Phys. Rev. Res. **5**, 013221 (2023).

[62] C. Genes, D. Vitali, and P. Tombesi, Emergence of atom-light-mirror entanglement inside an optical cavity, Phys. Rev. A **77**, 050307(R) (2008).

[63] S. Weis, R. Rivière, S. Deléglise, E. Gavartin, O. Arcizet, A. Schliesser, and T. J. Kippenberg, Optomechanically induced transparency, Science **330**, 1520 (2010).

[64] H. Xiong and Y. Wu, Fundamentals and applications of optomechanically induced transparency, Appl. Phys. Rev. **5**, 031305 (2018).

[65] S. Singh, M. Asjad, and C. R. Ooi, Tunable optical response in a hybrid quadratic optomechanical system coupled with single semiconductor quantum well, Quantum Inf. Proc. **21**, 47 (2022).

[66] H. Pan, Y. Yang, Z. An, and C.-M. Hu, Bistability in dissipatively coupled cavity magnonics, Phys. Rev. B **106**, 054425 (2022).

[67] J. Li and S. Gröblacher, Entangling the vibrational modes of two massive ferromagnetic spheres using cavity magnomechanics, Quantum Sci. Technol. **6**, 024005 (2021).

[68] C. Gardiner and P. Zoller, *Quantum Noise: A Handbook of Markovian and non-Markovian quantum Stochastic Methods with Applications to Quantum Optics* (Springer, Berlin, 2004).

[69] C. Ciuti and I. Carusotto, Input-output theory of cavities in the ultrastrong coupling regime: The case of time-independent cavity parameters, Phys. Rev. A **74**, 033811 (2006).

[70] S. Barzanjeh, E. Redchenko, M. Peruzzo, M. Wulf, D. Lewis, G. Arnold, and J. M. Fink, Stationary entangled radiation from micromechanical motion, Nature (London) **570**, 480 (2019).